IEEE Photonics Journal
An IEEE Photonics Society Publication

Open Access

Femtosecond Pulse Compression With Pedestal Suppression in a Sagnac Interferometer Constructed of Anti-Resonant Hollow Core Fiber

Volume 13, Number 2, April 2021

Taoying Yu
Xuesong Liu
Andrey D. Pryamikov
Alexey F. Kosolapov
Zhongwei Fan

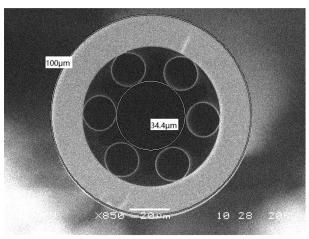

(a)

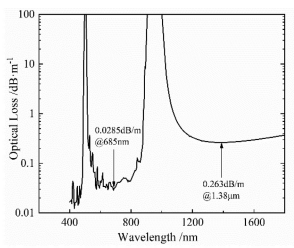

(b)

DOI: 10.1109/JPHOT.2021.3067891

Femtosecond Pulse Compression With Pedestal Suppression in a Sagnac Interferometer Constructed of Anti-Resonant Hollow Core Fiber

Taoying Yu,[1,2,3] **Xuesong Liu**,[1,2] **Andrey D. Pryamikov**,[4] **Alexey F. Kosolapov**,[4] **and Zhongwei Fan**[1,2,3]

[1]Aerospace Information Research Institute, Chinese Academy of Science, Beijing 100094, China
[2]National Engineering Research Center for DPSSL, Beijing 100094, China
[3]University of Chinese Academy of Sciences, Beijing 100094, China
[4]Prokhorov General Physics Institute, Russian Academy of Science, Moscow 119333, Russia

DOI:10.1109/JPHOT.2021.3067891

Manuscript received January 31, 2021; revised March 17, 2021; accepted March 18, 2021. Date of publication March 23, 2021; date of current version April 14, 2021. This work was supported in part by a Group of Short Pulse Laser Technology (GJJSTD20200009) and in part by the National Natural Science Foundation of China under Grant 61605215. Corresponding authors: Xuesong Liu; Zhongwei Fan (e-mail: b52sjtu@hotmail.com; fanzhongwei@aoe.ac.cn).

Abstract: In this paper, compression of high-power femtosecond pulses in Sagnac interferometers constructed of anti-resonant hollow core fibers (ARHCF) is investigated numerically and experimentally. By varying the types and pressures of gas filled in the hollow core fiber, the group velocity dispersion and the nonlinear pulse phase accumulation difference between clockwise and counterclockwise propagations could be tuned conveniently. In experiment, we demonstrate the pedestal suppression temporal pulse compression of 800 nm, 160 fs, 10 μJ pulses from a Ti: Sapphire laser at 1 kHz to 20 fs with maximum compression efficiency of 25% nearly and compression ratio of eight.

Index Terms: Pulse compression, pedestal suppression, Sagnac interferometer, anti-resonant fiber.

1. Introduction

Energetic ultrashort pulses are increasingly being sought in the past two decades, for many areas such as strong-field physics [1], high-order harmonic generation [2] and particle acceleration, etc. Mode-locking technique is a typical method to generate femtosecond pulse in the form of soliton [3] directly that have been investigated extensively. Different modulated media including nonlinear polarization rotation (NPR), semiconductor saturable absorber mirrors (SESAMs) and other 2D nanomaterials [4]–[5] like graphene, black phosphorus attracted extensively attentions. However, it's impossible to generate few-cycle laser pulses directly from the low-damage-threshold and limited-gain-bandwidth laser media and modulated media, leading to pulse compression techniques investigated intensively in past years. The compressed ultrashort pulses can be used in various applications, such as measurements of ultrafast physical process [6], surface science [7], and ultrahigh-data-rate communications [8] and so on.

Types of compression techniques based on silicon fibers in the nJ-level input [9] have been extensively investigated, especially two methods are mostly used. The first one is broadening spectrum by the Kerr nonlinear effect, i.e., self-phase modulation (SPM) in normally dispersive bulk materials [10] or fibers [11], and then compressing the pulses by external dispersive compensation, e.g., by grating pairs. However, the peak power is limited to the order of MWs, owing to material damage and self-focusing issues [12]. Moreover, the low coupling efficiency to small-core-diameter fibers and the diffractive loss of external free-space dispersive compensation would attenuate the compressed pulse energy further. The other approach is based on the soliton-effect compression (SEC) technology that combines effects of the SPM and the anomalous group velocity dispersion (GVD). In this method, no external dispersion compensation process is needed. Compared with external compression technique, SEC has advantages of compact structure, low diffraction loss; and moreover, it is a promising way to compress pulses down to few-cycle scales [13]. However, generally high compression ratio and high pulse contrast could not be achieved simultaneously in the both methods [14]. Though the adiabatic soliton compression in dispersion decreasing fibers (DDF), is able to meet the pulse contrast requirement, still suffers from long fiber length, i.e., more than hundreds of meters, and low compressed ratio. The high compression ratio could be achieved in a shorter length of fiber if the input soliton order is high, but the unbalance between GVD and nonlinearity will lead to severe pulse wings in the output pulse waveforms. On the other hand, the nonlinear optical loop mirror (NOLM) [31]–[32], or named as the Sagnac interferometer has been proved to be a very useful alternative scheme that can filter pulse pedestals [15]. The Sagnac or NOLM compression method have an obviously advantages of high compression ratio and clean pedestal. In the SEC, the low order soliton compression could achieve clean pedestal but low compression ratio for weak nonlinear chirp effect, while the high order soliton compression might achieve high compression ratio but suffer from soliton fission and strong pedestal issues for unbalance of strong nonlinear effect and weak dispersion compensation. Although the interferometer has increased the system's complexity and cost, especially the twice space light coupling into the fiber, the efficiency is decreasing to a certain too. It still provides a good reference for some special applications which needs high compression ratio and clean pedestal simultaneously.

Anti-resonant hollow core fiber (ARHCF) is a new kind of hollow core fibers emerged in recent years [16]–[18]. Thanks to the ultra-low transmission loss, flexible nonlinearity, tailorable dispersion, freedom to control the gas filled in the fiber [19], it is particularly suitable for delivery and compress high-peak-power ($>$2 GW [9]) ultrashort pulses [20]–[24]. [30] have achieved μJ-level pulses compression from 250 fs to sub-10 fs pulse using gas-filled Kagome-structured hollow-core photonic crystal fiber in two compressed stages, combined with the two aforementioned compression techniques. However, the output compressed pulse waveform present clear pedestals, and the peak power of the pre-pulse reached nearly 20% of the main pulse.

To achieve high-peak-power ultrashort pulse compression, especially with pedestal suppression and high compression ratio, the Sagnac interferometer based on ARHCF is investigated in this paper. ARHCF was filled with Argon so that the pulse evolution would not be affected by the stimulated Raman scattering (SRS) effect. By adjusting the pressure, gas dispersion and nonlinear coefficients could be tailored flexibly. We analyzed the pedestal-suppression pulse compression in the ARHCF interferometer with unbalanced splitting ratio between the clockwise and counter-clockwise directions. In experiment, we realized input pulse pedestal-suppression compression of 20 μJ, 160 fs pulses at 800 nm wavelength to output of 20 fs using 50 cm ARHCF.

2. Anti-Resonant Hollow Core Fiber

ARHCFs are highly promising for high-power ultrashort pulse applications, owing to their guiding mechanism and flexible gas filling characteristics. The anti-resonant reflecting optical waveguide model (ARROW) [25] explains that the ARHCF allows for several broad transmission bands with low loss, distributed from visible to mid-infrared spectrum. Filling with gas, instead of silicon in the core region provides a much higher material damage and self-focus threshold, as high as several GWs of peak power [9]. The low and adjustable dispersion characteristics by varying gas types and

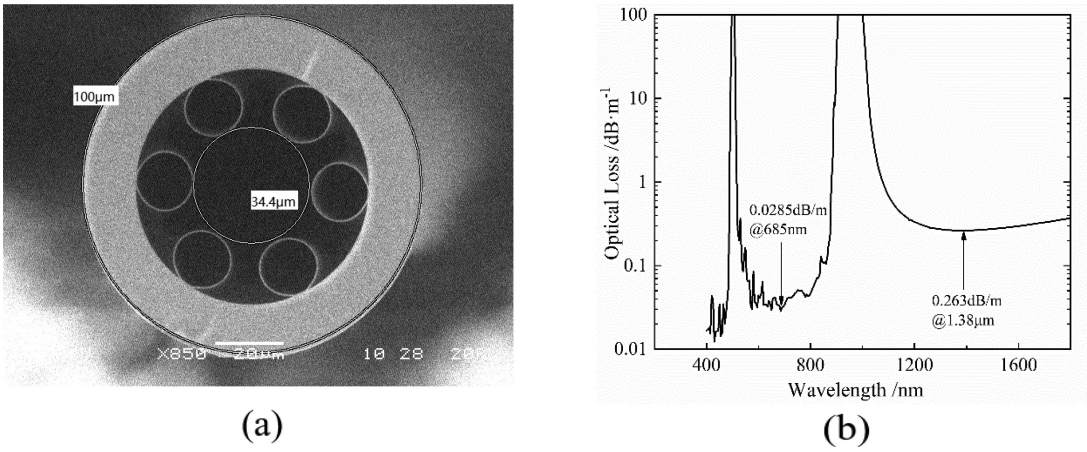

Fig. 1. (a) Scanning electron micrograph of ARHCF with a 34 μm core diameter. (b) Measured attenuation curves of the ARF. The high loss at ~500 nm and ~1000 nm is caused by the resonant coupling between the core mode and the cladding modes.

pressure make it suitable for high-peak-power ultrashort pulse delivery and high-order nonlinearity applications.

Fig. 1(a) shows the near field micrograph of the ARHCF used in this experiment, consisting of six untouched hollow cladding tubes for low loss at range of 500 nm to 850 nm and 1.2 μm to 1.7 μm, with minimum attenuation of 0.0285 dB/m and 0.263 dB/m, relatively. The outer diameter of the fiber is 100 μm while the cladding tube diameter is 16.25 μm; the corresponding strut thickness is estimated to be 400 nm and the core diameter is 34 μm. The core diameter leads to relatively small effective modal area, resulting in high peak power intensity for realizing the nonlinear process compared with other large core diameter ARF, moreover the small diameter would eliminate the high-order mode in the fiber. This would benefit for the Sagnac interferometer experiment.

A maximum coupling efficiency of 55% was achieved when an aspheric lens with 50 mm focal length was used to couple the Ti: Sapphire laser into the fiber. The 800 nm laser with 7 mm diameter could be focused to nearly 35 μm diameter. The attenuation of the fiber is measured from 400 nm to 1.6 μm by the cut-back method. Fig. 1(b) shows the attenuation curve measured in the fiber. A high loss region appears around 500 nm and 1 μm, corresponding to modes leaked from core into cladding strut.

The dispersion coefficients could be evaluated according to [26].

$$\beta_{mn} \approx k_0 \sqrt{\left(1 + \frac{p}{p_0}\frac{T_0}{T}\right)\delta(\lambda) - \left(\frac{u_{nm}}{ka}\right)^2} \tag{1}$$

where p is the gas pressure and T is the temperature in the chamber, $\delta(\lambda)$ is the Sellmeier expansion coefficient and k_0 is wave vector determined at $p_0 = 1$ bar and $T_0 = 253$ K; u_{nm} is the m^{th} root of the $(n-1)^{th}$ order Bessel function, k is the wave vector and a is the radius of the core. When the fiber is filled with Argon, the dispersion distributions with varied pressures are shown in Fig. 2. Meanwhile, the nonlinearity predominantly comes from the filled gas, rather than silicon fibers, because over 99% core mode field is confined in the hollow core. The nonlinearity coefficient γ of ARHCF with 34 μm core diameter, filled with 10 bar Ar gas is estimated to be $\sim 1 \times 10^{-6}$ m^{-1}W^{-1} [27].

3. Numerical Model

Fig. 3 shows the basic configuration of a Sagnac interferometer, consisting of an ARHCF shown in Fig. 1 and an α: (1-α) (α is a number from the range of 0 and 100) beam splitter (BS) with the

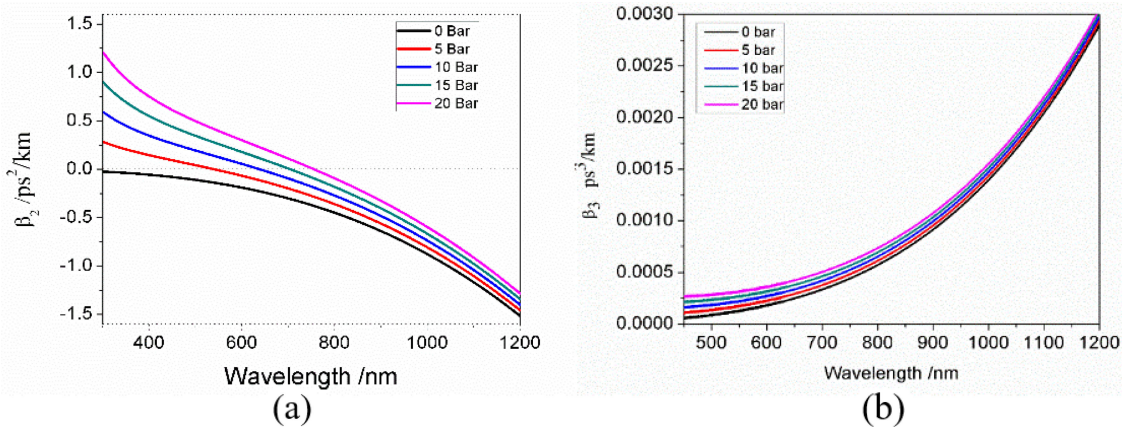

Fig. 2. Calculated dispersion distributions of the ARHCF with varied pressure of filled Ar. (a) Second-order dispersion coefficient; (b) Third-order dispersion coefficient.

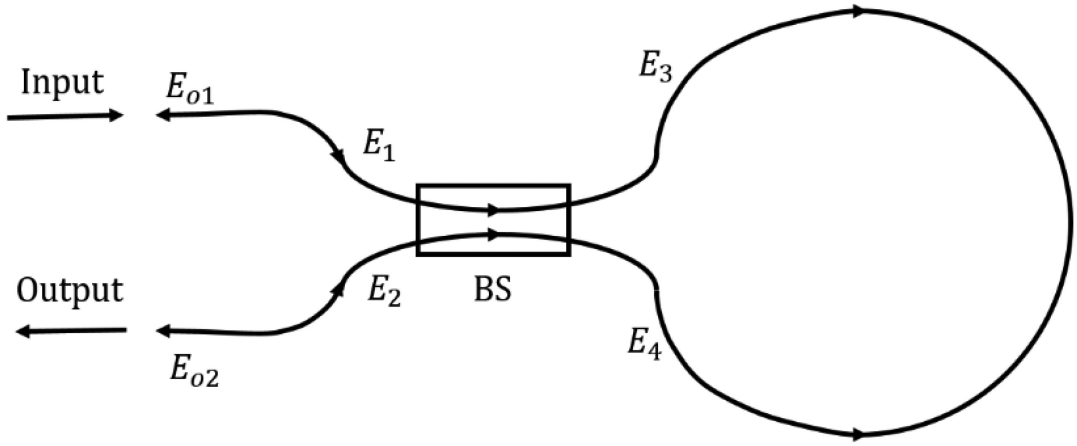

Fig. 3. The Sagnac interferometer configuration.

α% input propagating along the clockwise direction, while the other (1-α)% in counter-clockwise direction. The output E_{02} are obtained through the transmission of the Sagnac interferometer. The clockwise U and counter-clockwise V split pulses are:

$$\begin{cases} U = \sqrt{\alpha}\, u_1 \\ V = \sqrt{1-\alpha}\, u_1 \end{cases}. \tag{2}$$

Where u_1 is the input field amplitude of E_1, and U and V are the respective field amplitudes of E_3 and E_4. For the femtosecond laser input with tens of micro joules, the peak power is in the order of hundreds of MW, so that the nonlinearity such as SPM and cross-phase modulation (XPM) must be taken into account. In this case, the coupled nonlinear Schrodinger equations can be written as:

$$\begin{cases} \frac{\partial U}{\partial z} = -\frac{i\Delta\beta}{2}\frac{\partial U}{\partial t} - \frac{i\beta_2}{2}\frac{\partial^2 U}{\partial t^2} - \frac{i\beta_3}{6}\frac{\partial^3 U}{\partial t^3} + \frac{2}{3}i\gamma\left(|U|^2 + 2|V|^2\right)U \\ \frac{\partial V}{\partial z} = \frac{i\Delta\beta}{2}\frac{\partial V}{\partial t} - \frac{i\beta_2}{2}\frac{\partial^2 V}{\partial t^2} - \frac{i\beta_3}{6}\frac{\partial^3 V}{\partial t^3} + \frac{2}{3}i\gamma\left(|V|^2 + 2|U|^2\right)V \end{cases} \tag{3}$$

$$\gamma = n_2\omega/cA_{eff} \tag{4}$$

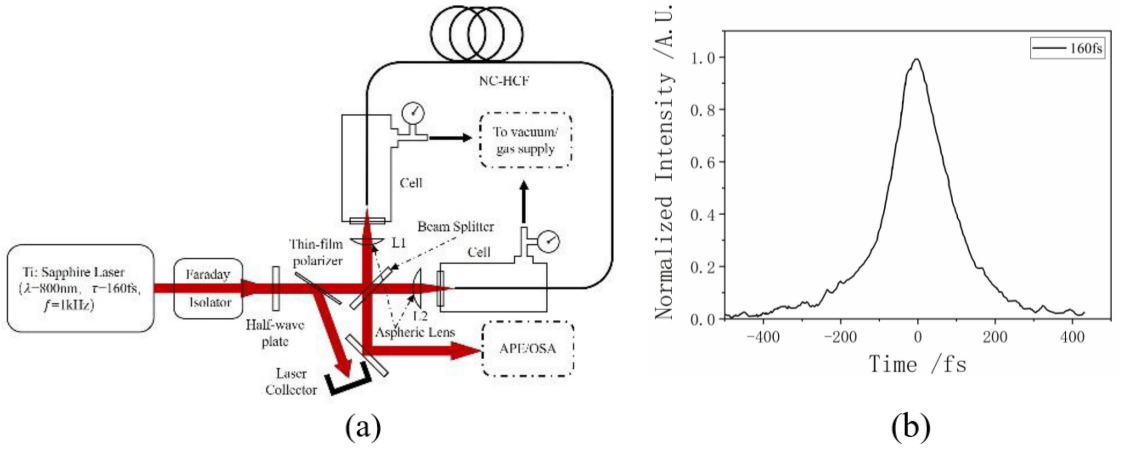

Fig. 4. (a) Schematic of the experimental setup; fs Laser: center wavelength of 800 nm, pulse duration of nearly ∼160fs; The focal length of the aspheric lens is 50.8 mm. (b) The autocorrelation curve of the input fs laser.

Where $\Delta\beta$ is the inverse group velocity mismatch, β_2, β_3 are the second-order and third-order dispersion parameters and γ is the Kerr nonlinear coefficient, n_2 is the pressure-dependent nonlinear refractive index of gas, ω the angular frequency and A_{eff} the effective area of the core. SRS are neglected because noble gas is filled in the fiber, and for and the fiber length is as short as of tens of centimeters. The equations could be calculated by the well-known split step Fourier method (SSFM). In each step the nonlinear and dispersion effect could be contributed to pulse evolution separately when the step size is small enough. An ordinary differential equation solver based on Runge-Kutta method could be used to solve the equation in each step. It could achieve 3rd order truncation error for ode45 function has been used.

4. Experiment Setup

A schematic of the experimental setup can be shown in Fig. 4(a). The Ti: Sapphire laser system (Spitfire, Spectra-Physics) was used as femtosecond pulse source, providing 160 fs pulses with energy up to 300 μJ, 800 nm central wavelength and 1 kHz repetition rate. The autocorrelation trace of the input fs pulses is shown in Fig. 4(b). A Faraday isolator (FI) was used to avoid the backward reflected light from the Sagnac interferometer. A half-wave plate (HWP1) and a thin film polarizer (TFP) were used to control the input power of linearly polarized pulses in range of several nJ to 20 μJ. A beam splitter (BS) with different splitting ratio, separates the input beam into two opposite-propagation beams. The transmitted and the reflected beam were separately focused by two identical aspherical lenses and coupled into the two ends of the ARHCF. An individual beam transmission efficiency could reach nearly 55%, including the coupling and ARHCF transmission loss. Two gas chambers were placed on both sides of the ARHCF to provide given dispersion and nonlinear environment. In chambers, different gas could be filled into the fiber with adjustable pressure. The ARF used is a symmetrical structure and the transmission is unsensitive to the polarization of input beam. Few polarization control devices after the beam splitter are used. In this experiment, 5∼10 bar Argon was pumped into the chambers. Fiber was coiled with a radius of approximately 30 cm to filter out possible high-order core modes. The clockwise and counter-clockwise propagating laser beams are recombined at the BS, and were split by the BS again, wherein one part was returned to the input direction, and the other part was defined as the output of the Sagnac interferometer, monitored by optical analyzers. Because of different split ratio in the clockwise and the counter-clockwise propagation beams, the two beams accumulate

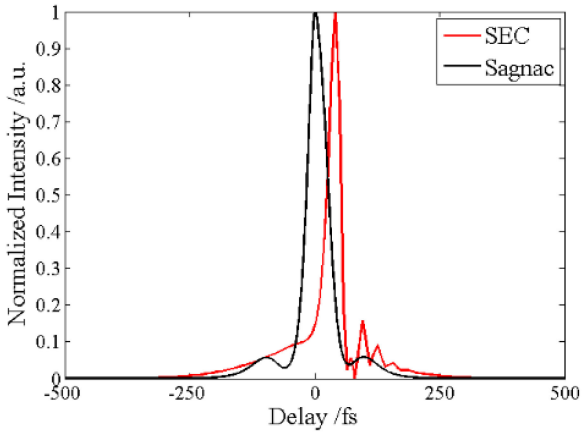

Fig. 5. Calculation results comparison with SEC and Sagnac interferometer compression.

different nonlinear phase shift along the fiber and generate interference effect when they are recombined at the BS. The overall result behaves as the transmission change of the Sagnac interferometer depending on the input power and the beam splitting ratio. With a selected beam splitting ratio, the transmittivity will increases with a span of input power. Within a pulse regime, the high instantaneous power part, i.e., near the peak part of a pulse, has higher transmission than the wing part far from the peak, which means the Sagnac interferometer can compress an input pulse. Moreover, since the peak power of a main pulse is higher than that of pulse pedestal (or wings) induced after the propagation in a length of ARHCF, the power contrast between pulse peak will be significantly enhanced, manifesting as the pedestal suppression by the Sagnac interferometer. An auto-correlator (APE pulse check) was used to measure the pulse states from the transmission port.

5. Results and Discussion

It is known that the high-order SEC would lead to inevitable pedestal and sub-pulse after a certain of propagation distance, as shown in Fig. 5. The red line depicts the temporal output of the 160 fs pulse after propagation in 50 cm ARHCF by the effect of SEC, computed by the generalized nonlinear Schrödinger equation (GNLSE) code [28]–[29]. The black line shows the output of Sagnac interferometer constructed of 50 cm fibers with identical gas environment with 55:45 beam split ratio. The pulse compressed with pedestal suppression has been achieved, compared with obviously sub-pulse as in the SEC scheme.

Ref. [8] has studied the properties of the Sagnac interferometer with varied loop length, gain, splitting ratio, input peak power, shape and frequency chirp of input pulses. However, varying gas pressure in hollow fibers is quite different from the situations in silicon-core fibers. Experiments in [8] just investigated the dispersion and nonlinear coefficient variations separately, whereas varying pressure could change both of coefficients simultaneously. The dispersion coefficient would be changed with pressure in Eq. (1) and Eq. (4).

According to Fig. 2(a), the absolute value of second-order dispersion drops with increasing pressure, whereas the nonlinear coefficient is growing at the same time. The output of the interferometer is the result of the interplay of linear phase shift induced by dispersions and nonlinear phase shift induced by SPM/XPM. The calculation result under different pressures can be seen in the Fig. 6. A transform-limited input pulse with 800 nm wavelength, 160 fs duration and 13 μJ energy was split by a 55:45 BS and coupled into the interferometer separately. As shown in Fig. 6, the temporal output shows periodic evolution, and the output amplitude grows with pressure increasing monotonically at the range from 5 bar to 10 bar. With

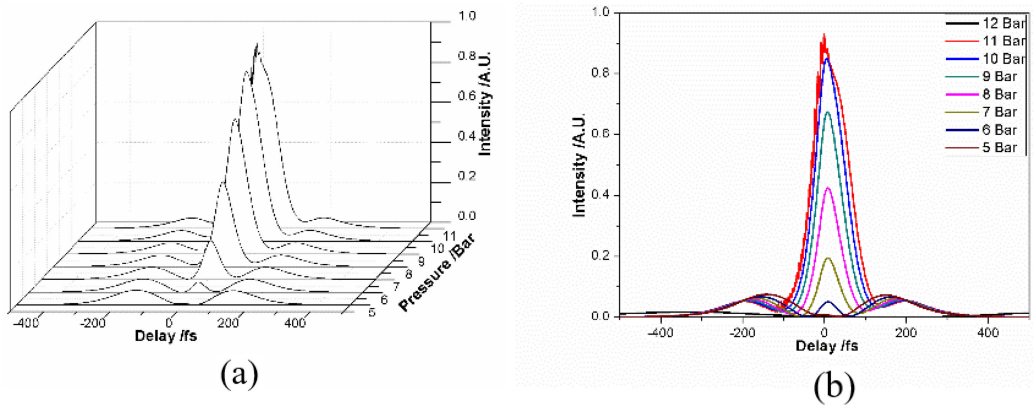

Fig. 6. Calculated temporal pulse shape in different pressure; (a) waterfall form and (b) point diagram.

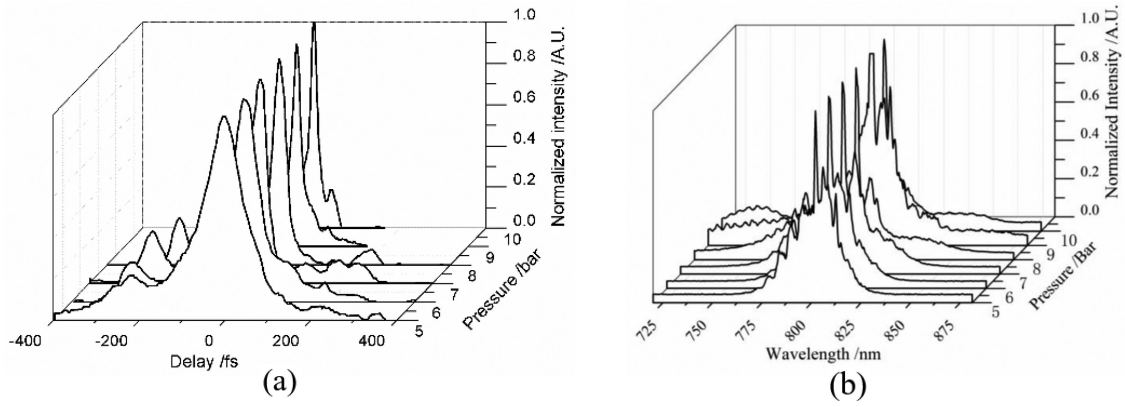

Fig. 7. The experimental output of (a) temporal evolution and (b) spectral evolution in Sagnac interferometer with varied pressures.

pressure rising, the compression efficiency (the ratio of energy of the pulse energy before and after compression) rises step by step and reached 25% maximum nearly. This relatively low compression efficiency results from twice coupling from laser into ARF and partial reflection from Sagnac interferometer. By coupling efficiency increasing the issues could be improved. According to Eq. (4), γ is small in the low pressure and the nonlinear phase modulation is small under low pressure. At the low pressure under 5 bar, the output of interferometer shows relatively large pedestal while main pulse, which is compressed a little for small nonlinear coefficient, had been reflected back to the FI. With pressure growing, the nonlinear coefficient γ rises and increased nonlinear phase chirp broaden the pulse spectrum. At the same time pulse was compressed through anomalous dispersion compensation and transmitted while the pedestal was reflected by the system. With pressure further rising, dispersion effect was playing little role on compensating the chirp whereas the nonlinear chirp strongly distorted the pulse. According to calculations, the pulse fission occurs when the pressure is beyond 11 Bar.

Fig. 7 depicted the corresponding experimental results of the Sagnac interferometer with ARHCF in different pressures. Fig. 7(a) shows the temporal evolution of the compressed pulse while Fig. 7(b) is spectral evolution. It is visible the onset of spectral broadening happens at pressures above 5 bar, and expanding from 750 nm to 850 nm for pressures nearly at 10 bar. At the same time the pulse duration decreases monotonically with pressure increasing from 5 bar to 10 bar,

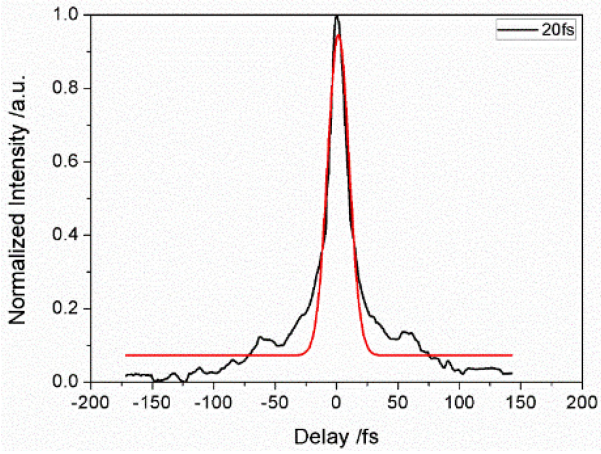

Fig. 8. The autocorrelation curve of Sagnac interferometer's output with Ar at 10 bars.

especially the pedestal is effectively suppressed above 7 bar. It's in good agreement with the calculated results showed in Fig. 6.

According to the parameters of fibers and gas environment, the optimal output could be achieved near 10 bars filling in the interferometer shown in Fig. 8. The dark line is the autocorrelation curves of the measured compressed pulse waveform and the red one is the fitting curve. The pulse in 20 fs width with suppressed pedestal suppression and 8 times compression ratio have been achieved in the Sagnac interferometer constructed of 50 cm ARHCF filled with Ar at 10 bars.

6. Conclusion

In conclusion, we have demonstrated a pedestal-suppression femtosecond pulse compression by a Sagnac interferometer constructed of AR-HCF numerically and experimentally. The anomalous GVD and nonlinear phase shift between the opposite directional propagating pulses could be adjusted conveniently by varying the pressure of gas filling in the fiber. With Ar at 10 bars filled, a pulse with 160 fs, 10 μJ pulse at 1 kHz repetition rate emitted from the Ti: Sapphire laser was compressed with the Sagnac interferometer. We have measured a compressed pulse duration of 20 fs with no obviously pedestal. The maximum compression efficiency is nearly 25%.

Given the results presented in this paper, we believe the configuration of Sagnac interferometer constructed of anti-resonant fiber is ideally suited for high signal-to-noise compression of high-power femtosecond laser. The compression technique is not only suitable for 800 nm laser, but also could be used in other wavelength if it could achieve the balance of dispersion and nonlinear effect. It's a promising way to achieve few-cycle compression through high order dispersion and nonlinear coefficients management carefully.

Acknowledgment

The authors wish to thank the Technical institute of Physics and Chemistry in Chinese Academy of China providing femtosecond laser.

References

[1] P. Colosimo *et al.*, "Scalling strong-field interations towards the classical limit," *Nat. Phys.*, vol. 4, pp. 386–389, 2008.
[2] P. Agostini and L. F. DiMauro, "The physics of attosecond light pulses," *Rep. Prog. Phys.*, vol. 67, pp. 813–855, 2004.
[3] Y. F. Song, X. J. Shi, C. F. Wu, D. Y. Tang, and H. Zhang, "Recent progress of study on optical solitons in fiber lasers," *Appl. Phys. Rev.*, vol. 6, no. 2, 2019, Art. no. 021313.

[4] M. Zhang *et al.*, "2D Black phosphorus saturable absorbers for ultrafast photonics," *Adv. Opt. Mater.*, vol. 7, no. 1, 2019, Art. no. 1800224.
[5] J. S. He, L. L. Tao, H. Zhang, B. Zhou, and J. B. Li, "Emerging 2D materials beyond graphene for ultrashort pulse generation in fiber lasers," *Nanoscale.*, vol. 11, pp. 2577–2593, 2019.
[6] R. Kienberger *et al.*, "Atomic transient recorder," *Nature*, vol. 427, no. 6977, pp. 817–821, 2004.
[7] E. Magerl *et al.*, "A flexible apparatus for attosecond photoelectron spectroscopy of solids and surface," *Rev. Sci. Instrum.*, vol. 82, no. 6, 2011, Art. no. 063104.
[8] P. K. A. Wai and W. H. Cao, "Simultaneous amplification and compression of ultrashort solitons in an Erbium-doped nonlinear amplifying fiber loop mirror," *IEEE. J. Quantum Electron.,* vol. 39, no. 4, pp. 555–561, Apr. 2003.
[9] K. F. Mak, J. C. Travers, N. Y. Joly, A. Abdolvand, and P. St. J. Russell, "Two techniques for temporal pulse compression in gas-filled hollow-core kagomé photonic crystal fiber," *Opt. Lett.*, vol. 38, no. 18, pp. 3592–3595, 2013.
[10] C. Rolland and P. B. Corkum, "Compression of high-power optical pulses," *J. Opt. Soc. Amer. B.*, vol. 5, pp. 641–647, 1988.
[11] W. J. Tomlinson, R. H. Stolen, and C. V. Shank, "Compression of optical pulses chirped by self-phase modulation in fibers," *J. Opt. Soc. Amer. B.*, vol. 1, pp. 139–149, 1984.
[12] G. P. Agrawal, *Nonlinear Fiber Optics*, Cambridge, MA, USA: Academic, 2007.
[13] J. C. Travers, W. Chang, J. Nold, N. Y. Joly, and P. St. J. Russell, "Ultrafast nonlinear optics in gas-filled hollow-core photonic crystal fibers [Invited]," *J. Opt. Soc. Amer. B.*, vol. 28, no. 12, pp. A11–A26, 2011.
[14] M. D. Pelusi and H. F. Liu, "Higher order soliton pulse compression in dispersion-decreasing optical fibers," *IEEE J. Quantum Electron.*, vol. 33, pp. 1430–1439, 1997.
[15] K. Smith, N. J. Doran, and P. G. J. Wigley, "Pulse shaping, compression, and pedestal suppression employing a nonlinear-optical loop mirror," *Opt. Lett.*, vol. 15, no. 22, pp. 1294–1296, 1990.
[16] A. D. Pryamikov, A. S. Biriukov, A. F. Kosolapov, V. G. Plotnichenko, S. L. Semjonov, and E. M. Dianov, "Demonstration of a waveguide regime for a silica hollow-core microstructured optical fiber with a negative curvature of the core boundary in the spectral region $>$3.5 μm," *Opt. Exp.*, vol. 19, no. 2, pp. 1441–1448, 2011.
[17] F. Yu, W. J. Wadsworth, and J. C. Knight, "Low loss silica hollow core fibers for 3–4 μm spectral region," *Opt. Exp.*, vol. 20, no. 10, pp. 11153–11158, 2012.
[18] A. N. Kolyadin, A. F. Kosolapov, A. D. Pryamikov, A. S. Biriukov, V. G. Plotnichenko, and E. M. Dianov, "Light transmission in negative curvature hollow core fiber in extremely high material loss region," *Opt. Exp.*, vol. 21, no. 8, pp. 9514–9519, 2013.
[19] F. Yu and J. Knight, "Negative curvature hollow core optical fiber," *IEEE J. Sel. Top. Quantum Electron.*, vol. 22, no. 2, Mar. 2016, Art. no. 4400610.
[20] A. N. Kolyadin *et al.*, "Negative curvature Hollow-core fibers: Dispersion properties and femtosecond pulse delivery," *Phys. Procedia.*, vol. 73, pp. 59–66, 2015.
[21] P. Jaworski, F. Yu, R. M. Carter, J. C. Knight, J. D. Shephard, and D. P. Hand, "High energy green nanosecond and picosecond pulse delivery through a negative curvature fiber for precision micro-machining," *Opt. Exp.*, vol. 23, no. 7, pp. 8498–8506, 2015.
[22] M. Gebhardt *et al.*, "Nonlinear pulse compression to 43 W GW-class few-cycle pulses at 2 μm wavelength," *Opt. Lett.*, vol. 42, no. 20, pp. 4179–4182, 2017.
[23] M. S. Habib, C. Markos, O. Bang, and M. Bache, "Soliton-plasma nonlinear dynamics in mid-IR gas-filled hollow-core fibers," *Opt. Lett*, vol. 42, no. 11, pp. 2232–2235, 2017.
[24] U. Elu *et al.*, "High average power and single-cycle pulses from a mid-IR optical parametric chirped pulse amplifier," *Optica*, vol. 4, no. 9, pp. 1024–1029, 2017.
[25] M. A. Duguay, Y. Kokubun, T. L. Koch, and L. Pfeiffer, "Antiresonant reflecting optical waveguides in sio2-Si multilayer structures," *Appl. Phys. Lett.*, vol. 44, no. 1, pp. 13–15, 1986.
[26] S. Im, A. Husakou, and J. Herrmann, "Guiding properties and dispersion control of kagome lattice hollow-core photonic crystal fibers," *Opt. Exp.*, vol. 17, no. 15, pp. 13050–13058, 2009.
[27] N. Y. Joly *et al.*, "Bright spatially coherent wavelength-tunable Deep-UV laser source using an ar-filled photonic crystal fiber," *Phys. Rev. Lett.*, vol. 106, no. 20, 2011, Art. no. 203901.
[28] A. Couairon *et al.*, "Practitioner's guide to laser pulse propagation models and simulation," *Eur. Phys. J-Spec. Topics*, vol. 199, no. 1, pp. 5–76, 2001.
[29] O. Pottiez, B. Ibarra-Escamilla, and E. A. Kuzin, "Large signal-to-noise enhancement of ultrashort pulsed optical signals using a power-symmetric nonlinear optical loop mirror with output polarization selection," *Opt. Fiber. Technol*, vol. 15, pp. 172–180, 2009.
[30] K. F. Mak *et al.*, "Compressing μJ-level pulses from 250 fs to sub-10 fs at 38-MHz repetition rate using two gas-filled hollow-core photonic crystal fiber stages," *Opt. Lett.*, vol. 40, no. 7, pp. 1238–1241, 2015.
[31] N. J. Doran and D. Wood, "Nonlinear-optical loop mirror," *Opt. Lett.*, vol. 13, no. 1, pp. 56–58, 1988.
[32] K. Smith, N. J. Doran, and P. G. J. Wigley, "Pulse shaping, compression, and pedestal suppression employing a nonlinear-optical loop mirror," *Opt. Lett.*, vol. 15, no. 22, pp. 1294–1296, 1990.